Journal of Computational Applied Mechanics 2025, 56(4): 838-862

DOI: 10.22059/jcamech.2025.398706.1552

RESEARCH PAPER

Surrogate-Assisted Peak-Slope Optimization of Dynamic Vibration Absorbers

Mahan Dashti Gohari [a], Mehdi Mohammadimehr [a, *], Ömer Civalek [b]

[a] *Department of Solid Mechanics, Faculty of Mechanical Engineering, University of Kashan, P.O. Box 87317-53153, Kashan, Iran*

[b] *China Medical University Hospital, China Medical University, Taichung, Taiwan*

Abstract

Dynamic vibration absorbers (DVAs) are widely used to mitigate resonant vibrations in mechanical systems by shifting the associated response peaks. However, optimizing their performance is computationally demanding, especially in systems with many degrees of freedom or numerous components, such as inerter-based DVAs. This study proposes a computationally efficient, surrogate-assisted optimization framework that leverages a novel Peak-Slope (PS) performance metric. As a reinterpretation of the classical H_∞ approach, the PS metric evaluates the effectiveness of vibration absorbers by measuring the secant slope between adjacent resonance peaks in the frequency response function. A well-tuned DVA yields a PS value approaching zero, indicating minimal variation between peaks and thus optimal mitigation of resonance. To reduce complexity, the structural parameters are held constant, and the influence of absorber parameters on the PS metric is isolated. The optimization space is simplified using surrogate models constructed via quartic polynomial regression. A novel decoupling algorithm introduced in this study enables efficient estimation of the PS metric as the Decoupled Peak-Slope (DPS) by expressing it as a sum of independent surrogate functions, each dependent on a single DVA parameter. Optimization is then performed by minimizing this total sum. A fully coupled 1DOF–1DOF system, incorporating masses, springs, dampers, and inerters, is used as the benchmark to validate the method. The DPS approach is compared against traditional genetic algorithm (GA)-based optimization, demonstrating substantial gains in both speed and accuracy. Further validation is conducted using reduced-order systems from the literature, confirming the true decoupling capability of the framework. For four distinct structural configurations, the decoupled surrogate equations are generated and summarized, forming a catalogue of precomputed polynomial functions that enables rapid evaluation of optimal DVA parameters across a range of systems. The results show strong agreement with analytical solutions and superior performance over GA-based methods. This positions the DPS framework as a fast, accurate tool for future semi-active DVA systems, enabling real-time tuning via precomputed surrogate functions.

Keywords: Dynamic Vibration Absorber (DVA), Surrogate Modelling, Peak-Slope Metric, Optimization, Decoupling Algorithm

[*] Corresponding author. Tel.: +98-31-55913432; fax: +98-31-5551-1121.
E-mail address: mmohammadimehr@kashanu.ac.ir

Nomenclature

Symbol	Definition	Units
β_p	Inerter ratio of the p-th absorber: $b_{a,p}/M$	—
λ_p	Stiffness ratio of the p-th absorber: $k_{a,p}/K_1$	—
μ_p	Mass ratio of the p-th absorber: $m_{a,p}/M$	—
ν_p	Damping ratio of the p-th absorber: $c_{a,p}/C_1$	—
ω_{dc}	Decoupled natural frequency: $\sqrt{(K_1/M)}$	rad/s
ω_i, ω_j	Resonance frequencies of the i-th and j-th peaks	rad/s
$\zeta_d c$	Decoupled damping ratio: $C_1/(2M\omega_{dc})$	—
$[F]$	Force vector including base excitation and external forces	N
K_1, C_1	Stiffness and damping of the host structure	N/m, Ns/m
M	Reference mass of the main system	kg
P	Number of dynamic vibration absorbers (DVAs)	—
$[M], [C], [K]$	Mass, damping, and stiffness matrices of the system	—
$b_{a,p}$	Inerter coefficient of the p-th absorber	kg
$c_{a,p}$	Damping coefficient of the p-th absorber	Ns/m
$k_{a,p}$	Stiffness of the p-th absorber	N/m
$m_{a,p}$	Mass of the p-th absorber	kg
q	Generalized displacement vector	m

1. Introduction

The presence of vibrations in mechanical systems is an inherent consequence of dynamic operations, frequently resulting in diminished performance, reduced precision, and accelerated structural degradation. To mitigate these adverse effects, the implementation of effective vibration control is regarded as essential for enhancing reliability and prolonging operational lifespan. Vibration control methodologies are typically categorized into passive and active systems. In passive control, energy dissipation is achieved through the inherent mechanical characteristics of materials and structures, utilizing devices such as tuned mass dampers (TMDs), viscoelastic layers, and isolation mounts. These techniques are widely favoured due to their structural simplicity, cost-efficiency, and long-term reliability under a broad range of operating conditions[1-3]. Active vibration control is characterized by the use of sensors, actuators, and real-time control algorithms to counteract vibrations through feedback or feedforward mechanisms. Adaptive and hybrid strategies have also been developed to extend the effectiveness of active systems across varying operational states. These methods are particularly advantageous in high-precision and dynamically variable environments, such as aerospace structures and advanced manufacturing platforms[4-6].

Dynamic Vibration Absorbers (DVAs), commonly referred to as tuned mass dampers (TMDs) in structural engineering, are passive devices designed to mitigate vibratory energy by introducing a secondary mass-spring-damper system. This system is tuned to, or slightly detuned from, the dominant natural frequency of the primary structure, effectively splitting the original resonance into multiple peaks and redistributing vibrational energy away from the main system. The foundational concept, patented by Frahm in 1909 [7], was rigorously analyzed in the seminal work of Ormondroyd and Den Hartog [8, 9]. Subsequent contributions by Bishop and Welbourn, as well as Brock, formalized practical tuning and damping methodologies, solidifying DVAs as an integral tool in machinery, civil infrastructure, and aerospace design [10, 11]. The advent of smart materials has greatly expanded the capabilities of vibration control, introducing semi-active and hybrid designs capable of real-time adjustments. Materials such as magnetorheological (MR) fluids, piezoelectric, and shape-memory alloys have transformed the landscape of vibration control, offering enhanced adaptability and multifunctionality. These innovations have found applications ranging from structural systems to high-precision industrial settings, marking a significant technological leap in vibration control [5, 12-29].

Classical fixed-point theory has traditionally assumed undamped single-degree-of-freedom (SDOF) systems as hosts, overlooking the complexities inherent in real-world structures. However, actual systems exhibit intrinsic damping, modal coupling, geometric nonlinearity etc. Early investigations addressing these phenomena began with Carter and Liu's pioneering study on nonlinear absorbers [30] and Thomson's development of viscously damped tuning charts [31]. These milestones paved the way for subsequent methodological advancements aimed at tackling the challenges posed by these structural complexities. Exact closed-form solutions for damped systems under H_∞ and

H_2 criteria were later introduced by researchers[32-34], providing robust frameworks for system tuning. These contributions were extended to accommodate multiple optimization criteria and detuned configurations [35-39]. Consequently, research began to emphasize multiple-tuned-mass-damper (MTMD) arrays and distributed networks capable of mitigating vibrations across a broader range of frequencies. Foundational work in modal interaction by Igusa and Xu [40], and Clarke [41] demonstrated that arrays comprising numerous smaller absorbers outperform single, large absorbers in terms of robustness and reliability. These studies laid the groundwork for subsequent advancements in geometric and topological optimization methodologies applicable to pipelines, towers, and rotating spacecraft [42-46].

Through these methodological innovations, the field has transitioned beyond the limitations of idealized SDOF models towards configurations capable of addressing multi-modal, non-linear, and distributed vibration problems effectively. Simultaneously, the necessity to mitigate broadband, low-frequency vibrations, especially in challenging applications such as spacecraft panels, vehicle chassis, and offshore risers, has driven the evolution of modelling approaches. Classical lumped SDOF models are steadily being supplanted by high-order continuous and hybrid formulations to address spatially distributed characteristics and multi-modal interactions in host structures [46-52]. These advanced models account for complex damping behaviours by incorporating distributed damping layers, Visco-elastic joints, and poroelastic materials, which have been shown to significantly enhance vibration attenuation under diverse operational constraints [53, 54].

Despite its theoretical appeal, H_∞ design remains computationally intensive, particularly when applied to high-order analytical models common in advanced vibration absorber systems. Its reliance on detailed analytical models makes the optimization process difficult and time-consuming. In practice, standard numerical methods often struggle with this complexity and tend to become stuck in suboptimal solutions, limiting the practical effectiveness of H_∞ design [55, 56].

DVAs are widely adopted for passive vibration control in engineering systems; however, optimizing their performance under realistic conditions remains a significant challenge. When complex features such as damping, inerters, and multi-modal coupling are introduced, traditional optimization methods, especially those based on classical and analytical methods, often lose effectiveness and robustness due to their high computational requirements. Moreover, conventional numerical techniques, including direct search and gradient-based methods, are frequently hampered by high computational costs, poor scalability, and difficulty in handling nonlinear or high-dimensional parameter spaces. While surrogate models have been explored to alleviate some of these issues, there is still a lack of dedicated, high-fidelity surrogate-assisted frameworks tailored to DVAs that can deliver both speed and precision. This gap limits the practical application of DVAs in complex structures where rapid, accurate optimization is essential.

To overcome the limitations of conventional DVA tuning approaches, this study introduces a surrogate-assisted optimization framework centered on a physically intuitive performance metric called the Peak-Slope (PS). The PS metric quantifies the slope between adjacent resonance peaks in a system's frequency-response function (FRF), providing a generalization of the classical equal-peak method used in vibration control. When the system is well-tuned, the PS value approaches zero, indicating balanced peak amplitudes and optimal energy distribution. To make the optimization process both fast and scalable, a new decoupling algorithm is developed. This algorithm expresses the overall PS value as a sum of independent, single-variable functions, each one corresponding to an individual absorber parameter (such as damping or stiffness). Instead of optimizing over a high-dimensional parameter space, the problem is simplified into a series of univariate surrogate models. These models are constructed using quartic polynomial regression, which is selected after testing several polynomial orders and shown to provide the best trade-off between accuracy and computational speed. Importantly, this decoupling targets only the absorber parameters, keeping the structural and excitation parameters fixed. This focused optimization, termed Decoupled Peak-Slope (DPS), transforms the original high-fidelity dynamic model into a set of simple polynomial expressions. The total PS can then be minimized by summing these expressions and searching for their optimal parameter values no full-system simulation is needed during the optimization stage. To demonstrate the method's effectiveness, the framework is validated on a fully coupled 1DOF–1DOF mechanical benchmark. Because the surrogate functions can be stored in compact polynomial form, this method is highly suitable for real-time or semi-active vibration absorber applications. Engineers can retrieve precomputed tuning curves for fast reconfiguration, enabling intelligent vibration control with negligible computational overhead. Visual examples, comparison plots, and tabular summaries included throughout the manuscript help clarify each step of the methodology and reinforce its practical value.

2. Methodology

2.1. The Peaks Slope (PS) criteria

According to the H_∞ criterion, a system achieves minimal response at resonance when the peaks of the Frequency Response Function (FRF) are of equal magnitude [57-62]. In the analysis of coupled linear dynamic systems, the FRF serves as a fundamental tool for characterizing the system's steady-state response to harmonic excitation across a continuous frequency range. In systems exhibiting multiple vibration modes, the FRF typically displays a series of distinct resonance peaks, each corresponding to a natural frequency and its associated response amplitude. To provide a consistent and quantitative measure of the amplitude variation between these resonant peaks, we introduce a novel scalar performance metric termed the Peak-Slope (PS). This metric captures the rate of change in amplitude between adjacent resonances and thereby offers an objective means of evaluating the balance and uniformity of the system's dynamic response. Importantly, the PS criterion is broadly applicable, enabling comparisons across systems with varying degrees of freedom, coupling characteristics, and absorber configurations. Its generality makes it especially suitable for surrogate-assisted optimization frameworks aimed at tuning dynamic vibration absorbers in both simple and complex structural systems.

2.2. General Definition of PS

Let A_i and A_j be the amplitudes of the i-th and j-th resonant peaks, respectively, and let ω_i and ω_j be their corresponding resonance frequencies, where $\mathrm{i} < \mathrm{j}$, and i, j belong to the set $1,2,\dots,\mathrm{N}$, with N denoting the total number of resonant peaks in the system. The Peaks Slope (PS) between the i-th and j-th peaks is defined as:

$$\mathrm{PS}_{i,j} = \frac{A_j - A_i}{\omega_j - \omega_i} \tag{1}$$

This expression represents the slope of the secant line that intersects the FRF magnitude curve at the two selected resonant peaks. It characterizes the rate of amplitude change per unit frequency between two resonance modes.

2.3. Matrix, Vector, and Scalar Form for Multiple Peaks

To capture the pairwise slope relationships between all resonant peaks in a symmetric fashion, the set of Peaks Slope values can be represented using a **skew-symmetric matrix PS** $\in R^{\mathrm{nxn}}$, where each entry $\mathrm{PS}_{\mathrm{ij}}$ corresponds to the Peaks Slope between the i-th and j-th resonance peaks. The PS matrix is defined as:

$$[PS] = \begin{bmatrix} 0 & PS_{12} & PS_{13} & & PS_{1N} \\ PS_{21} & 0 & PS_{23} & \cdots & PS_{2N} \\ PS_{31} & PS_{32} & 0 & & PS_{3N} \\ & \vdots & & \ddots & \vdots \\ PS_{N1} & PS_{N2} & PS_{N3} & \cdots & 0 \end{bmatrix} \tag{2}$$

Where:

$$PS_{\mathrm{ji}} = -PS_{\mathrm{ij}}, \quad \forall\, i \neq j \tag{3}$$

$$PS_{ij} = 0, \quad \forall i = j \tag{4}$$

In systems with more than two resonant peaks, organizing the pairwise Peak-Slope values into a vector, instead of using the full matrix, provides a more efficient and practical representation. This vector format significantly reduces computational and memory demands while retaining all critical information about the amplitude variations between each pair of resonance peaks. By preserving the essential dynamics of the system in a simplified structure, the vector form supports faster processing and easier integration into surrogate modelling and optimization procedures without sacrificing analytical depth or accuracy.

$$PS = \left[PS_{1,2}, PS_{2,3}, \dots, PS_{N-1,N}\right] \tag{5}$$

In practical applications where reducing complexity is essential, such as in optimization tasks or early design

stages a simplified scalar version of the PS metric can be employed. Instead of evaluating the full matrix or vector of slope values between all frequency peaks, this approach focuses on the maximum slope observed between adjacent dominant peaks in the FRF. This simplification captures the most critical imbalance in dynamic behaviour while avoiding the overhead of analysing the complete spectral structure. This scalar form maintains the essential physical interpretation of the PS metric: when the dominant peaks are well balanced, the slope approaches zero, indicating effective tuning of the dynamic vibration absorber. Conversely, large PS values indicate a mismatch in peak amplitudes and poor absorber performance. The compactness of this scalar form makes it especially well-suited for surrogate modeling and sensitivity analyses, where computational resources are limited or fast evaluations are needed. The scalar Peak-Slope is formally defined as:

$$\mathrm{PS}(\theta) = \max_{1 \le i < j \le N_p} \left| \frac{A_j(\theta) - A_i(\theta)}{\omega_j - \omega_i} \right| \tag{6}$$

2.4. Physical Interpretation and Theoretical Implications

The PS metric provides an intuitive and quantitative measure of imbalance in a system's frequency response, specifically targeting the asymmetry between adjacent resonance peaks in the FRF. When the PS value is close to zero, it indicates that the peaks have nearly equal amplitudes, an outcome associated with *optimal absorber tuning*, as it reflects a more uniform distribution of vibratory energy across the system. This condition is especially important in vibration mitigation applications, where minimizing the system's peak response amplitude is critical to improving performance and reliability. Conversely, larger PS values signal greater imbalance, suggesting potential issues such as poor parameter selection, misplacement of absorbers, or inefficient modal interactions. As such, PS serves not only as a tuning objective but also as a diagnostic indicator of absorber performance. From a theoretical standpoint, the PS metric can be seen as a practical reformulation of the classical H_∞, which is widely used in control theory to assess system robustness. However, unlike H_∞, which typically requires computationally expensive norm evaluations over frequency domains, the PS offers a simplified, localized scalar measure that is more computationally efficient and numerically stable key advantages for real-time or surrogate-based optimization.

Importantly, the PS metric is well-suited for use with surrogate models due to its smooth, continuous nature and its sensitivity to tuning parameters. This compatibility reduces the need to solve complex differential equations during every optimization iteration. Instead, the system's performance trends can be approximated using polynomial surrogates, dramatically accelerating the design process without compromising accuracy.

2.5. Decoupling of the PS Criterion

The design space for such systems is represented by a comprehensive parameter vector $\theta \in R^q$, which is partitioned into three mutually independent subspaces:

- The primary structural parameters, denoted θ_S, govern the physical architecture of the host structure. These include the masses m_i across each degree of freedom i, as well as the stiffness and damping interactions represented by k_{ij} and c_{ij}, respectively, between any two connected masses i and j. These parameters define the core dynamics of the structure without any absorbers attached.

- The absorber parameters, denoted θ_A, capture the characteristics of each attached dynamic vibration absorber. In a system compromising P DVAs, each absorber contributes a normalized mass ratio $\mu_p = \frac{m_{a,p}}{M}$, where $m_{a,p}$ is the p-th absorber mass and M is the reference mass of the primary system. Absorbers may also include inerters, represented by dimensionless ratios $\beta_p = \frac{b_{a,p,l}}{M}$, where $b_{a,p,l}$ is l-th inerter of the p-th DVA. The stiffness ratio is defined as $\lambda_p = \frac{k_{a,p,l}}{K_1}$, where $k_{a,p,l}$ is the l-th stiffness coefficient of the p-th DVA and K is a reference stiffness in the host structure. The damping ratio is given by $\nu_p = \frac{c_{a,p,l}}{C}$, where $c_{a,p,l}$ is l-th damper coefficient of the p-th DVA and C is a baseline damping coefficient.

- The excitation and environmental parameters, denoted θ_E, account for external forcing conditions and boundary movements. These include base excitation amplitudes A_{Low} and A_{up}, representing the

amplitude of harmonic motion applied at the lower and upper supports of the system, and the forcing magnitude F acting on the main structure. Additional parameters include the characteristic frequency $\omega_{dc} = \sqrt{\frac{K}{M}}$ derived from the main stiffness and mass, and the associated damping ratio $\zeta_{dc} = \frac{C}{2M\omega_{dc}}$, which captures the system's decay behavior in the absence of absorbers.

And thus, the design space can be written as:

$$\theta = \theta_S + \theta_A + \theta_E \tag{7}$$

Accordingly, an iterative additive surrogate is constructed, wherein the overall PS is reconstructed by successively fitting one-dimensional component functions. Let the absorber–design vector be defined as:

$$\eta^{(\mathrm{i})} = \left[\beta_1^{(\mathrm{i})}, \ldots, \beta_P^{(\mathrm{i})}, \lambda_1^{(\mathrm{i})}, \ldots, \lambda_P^{(\mathrm{i})}, \mu_1^{(\mathrm{i})}, \ldots, \mu_P^{(\mathrm{i})}, \nu_1^{(\mathrm{i})}, \ldots, \nu_P^{(\mathrm{i})}\right]^T \tag{8}$$

where each $\beta_p^{(\mathrm{i})}, \lambda_p^{(\mathrm{i})}, \mu_p^{(\mathrm{i})}$ and $\nu_p^{(\mathrm{i})}$ denotes, in normalized form, the inerter ratio, stiffness ratio, mass ratio, and damping ratio of the p-th element for the i-th set.

The PS function, which models the system response as a function of the full input vector, is defined as follows:

$$\mathrm{PS}(\eta) \coloneqq X(\eta) \tag{9}$$

Thus, the response is approximated as a sum of univariate component functions that is considered as:

$$DPS(\eta) \coloneqq \sum_{r=1}^{d} X_r(\eta) \tag{10}$$

The error function for each set of input values is written as:

$$\varepsilon^{(i)} = PS\left(\boldsymbol{\eta}^{(i)}\right) - DPS\left(\boldsymbol{\eta}^{(i)}\right) \tag{11}$$

The following algorithm is applied until $|\varepsilon^{(i)}|$ falls below a prescribed tolerance τ_{tol}:

1) Sampling grid selection: An m-point grid $\{\eta^{(1)}, \ldots, \eta^{(m)}\}$ is chosen uniformly over each coordinate's admissible interval.
2) Initialisation: All component functions are set to zero, $X_r^{(0)}(\eta) = 0$, so that $\mathrm{DPS}^{(0)} = 0$.
3) Outer iteration: For each coordinate index $r = 1, \ldots, R$ the following steps are performed:
   a) Outer iteration:
   A partial design vector is formed by fixing all other coordinates at reference values η^{ref} except for one parameter $\eta_{\mathrm{var}}{}^{(i)}$:

$$\boldsymbol{\eta_r^{(i)}} = \left[\eta_1^{\mathrm{ref}}, \ldots, \eta_{r-1}^{\mathrm{ref}}, \eta_{var}{}^{(i)}, \eta_{r+1}^{\mathrm{ref}}, \ldots, \eta_R^{\mathrm{ref}}\right]^{\mathsf{T}} \tag{12}$$

   b) The one-dimensional residual samples are then computed as

$$y_r^{(i)} = DPS^{(k)}\left(\eta_r^{(k)}\right) - \sum_{s=1,\ s\neq r}^{R} X_s^{(k)}\left(\eta_s^{\mathrm{ref}}\right), \quad i = 1, \ldots, m. \tag{13}$$

   c) Univariate fit: In this step, a regression procedure is performed to update the component function $X_r^{(k+1)}$ for the r-th coordinate direction. Given a set of m one-dimensional residual samples $\{\left(\eta_r^{(i)}, y_r^{(i)}\right)\}_{i=1}^{m}$, the goal is to find a function f within a suitable hypothesis space $\mathcal{H}_{\chi_r}$ (e.g., polynomials, radial basis functions,

splines, Gaussian processes) that best fits the residual data. This is achieved by solving the following regularized optimization problem:

$$DPS_r^{(k+1)} = \arg\min_{f \in \mathcal{H}_{X_r}} \left[\frac{1}{m} \sum_{i=1}^{m} \mathcal{L}\left(y_r^{(i)}\right) + \alpha\, \Omega(f) \right], \quad \alpha \geq 0 \tag{14}$$

where $\mathcal{L}\left(y_r^{(i)}\right)$ is a loss function (e.g. squared error, absolute error, Huber loss, log loss or etc.), $\Omega(f)$ is a regularization penalty (e.g. norm, total variation, smoothness penalty or etc.) ,and $\alpha \geq 0$ is a regularization coefficient enforcing smoothness or preventing overfitting.

Fig.1(a) presents a flowchart outlining the algorithm used to extract decoupled functions $DPS^{(k)}$ from a fully coupled dynamic system. The process begins by setting the parameters for the main system, the DVA, and the tolerance for the "Maximum Peak Slope." An input space is defined, followed by the computation of the peak slope values across this space. A decoupled functional form is then proposed and fitted using a selected method. The fitting accuracy is evaluated against the actual peak slope values. The algorithm iteratively refines the fit and input coverage until the fitting satisfies the tolerance, captures system complexity, and sufficiently spans the input space. Once validated as a reliable approximation of the full system, the decoupled functions are extracted. Figure 1(b) illustrates the overall process used to extract the optimal DVA parameters from the decoupled surrogate functions. The procedure begins by setting the values of the structural system parameters, excitation and environmental conditions, and the allowable range of DVA parameters for the fully coupled system. Using the surrogate-assisted algorithm introduced in Figure 1(a), the appropriate coefficient values for each decoupled DPS function are computed. The optimization is then carried out by minimizing the total sum of all $X(i)$ values, including those corresponding to fixed or zero parameters. The resulting set of DVA parameters that minimizes this summation is identified as the optimal configuration. Finally, this optimal parameter set is extracted for implementation or further analysis.

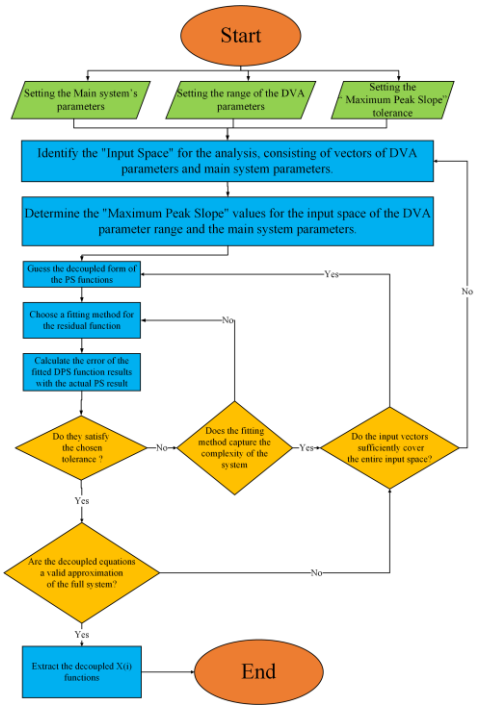

(a)

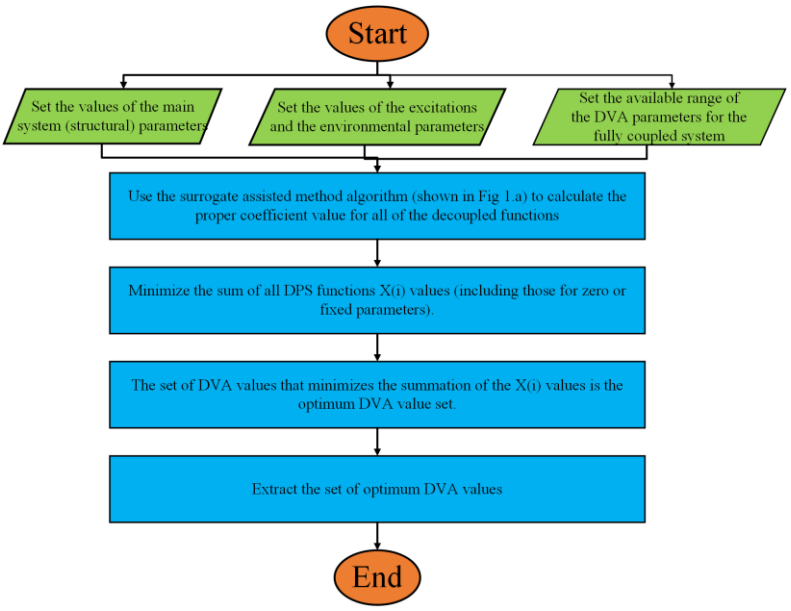

(b)

Figure 1. (a) Algorithm flowchart for extracting decoupled functions from a fully coupled system using peak slope analysis and model fitting. (b) Flowchart of the overall procedure used to determine the optimal DVA parameter set from the decoupled surrogate model, based on system, excitation, and design constraints.

3. Benchmark Analysis of a Fully Coupled 1DOF–1DOF System

3.1. System Overview and Configuration

To validate the proposed surrogate-assisted PS optimization framework, a fully coupled 1DOF–1DOF mechanical system has been selected as a comprehensive benchmark. This configuration is deliberately constructed to incorporate all fundamental elements typically found in vibratory structures: primary and secondary masses, springs, dampers, and inerters. The term *fully coupled* is used to emphasize that both the primary system and the DVA are not only interconnected with each other, but also jointly coupled to all supporting base nodes, ensuring a complete exchange of dynamic interactions. This benchmark system serves as a representative model for complex real-world applications, making it an ideal platform to demonstrate the core operational behaviour and benefits of the proposed algorithm. To enhance clarity, a schematic of the system layout is provided in Fig. 2, which visually illustrates the arrangement of components and their interconnections.

3.2. Mathematical Modelling of the System with Assumptions

The main system is modelled as a fundamental 1DOF structure consisting of a mass, springs, and dampers connected to upper and lower bases. Key assumptions include linear elastic behaviour (for stiffnesses K_1 andK_2), linear structural damping (for damping coefficients $C_1$and C_2), and purely translational motion, with rotational effects neglected. These assumptions enable a simplified yet accurate representation suitable for vibration analysis and control optimization. The upper and lower bases are modelled adaptively, either as additional masses in complex systems or as fixed foundations, depending on the application. The DVA is also represented as a 1DOF system incorporating masses, springs, dampers, and inerters, fully coupled with the main system and the bases. Its modelling assumptions mirror those of the primary structure.

Let q be the generalized coordinate of the system. The displacements of the main system and the DVA at time t are denoted by $U(t)$ and $u(t)$, respectively.

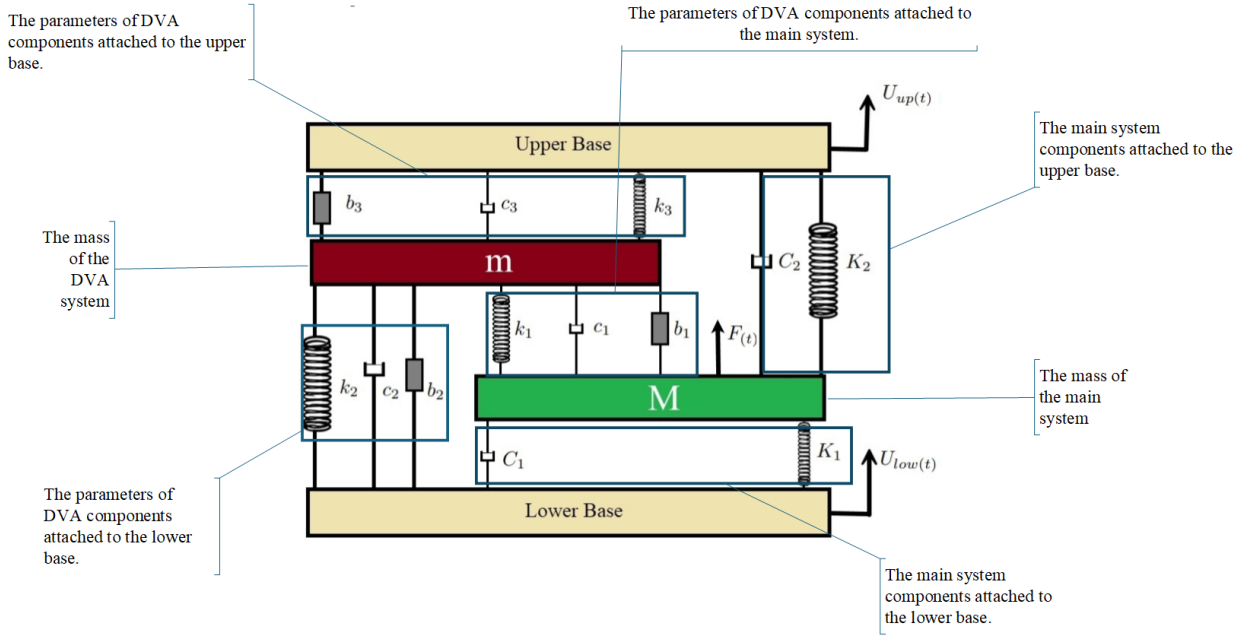

Figure 2: A schematic view for a fully coupled 1DOF - 1 DOF system

$$q = \begin{bmatrix} U(t) \\ u(t) \end{bmatrix}, \dot{q} = \begin{bmatrix} \dot{U(t)} \\ \dot{u(t)} \end{bmatrix}, \ddot{q} = \begin{bmatrix} \ddot{U(t)} \\ \ddot{u(t)} \end{bmatrix} \tag{15}$$

The equation of motion can be expressed using the dimensional parameters as:

$$[M][\ddot{q}] + 2\zeta_{dc}\omega_{dc}[C][\dot{q}] + \omega_{dc}^2[K][q] = [F] \tag{16}$$

where the mass, damping, spring matrices are considered as:

$$[M] = \begin{bmatrix} 1+\beta_1 & -\beta_1 \\ -\beta_1 & \mu+\beta_1+\beta_2+\beta_3 \end{bmatrix} \tag{17}$$

$$[C] = \begin{bmatrix} 1+N+\nu_1 & -\nu_1 \\ -\nu_1 & \nu_1+\nu_2+\nu_3 \end{bmatrix} \tag{18}$$

$$[K] = \begin{bmatrix} 1+\Lambda+\lambda_1 & -\lambda_1 \\ -\lambda_1 & \lambda_1+\lambda_2+\lambda_3 \end{bmatrix} \tag{19}$$

$$[F] = \begin{bmatrix} F' + 2\zeta_{dc}\omega_{dc}\left(\dot{U_{Low}} + N\dot{U_{Up}}\right) + \omega_{dc}^2\left(U_{Low(t)} + \Lambda U_{Up(t)}\right) \\ \beta_2\ddot{U_{Low}} + \beta_3\ddot{U_{Up}} + 2\zeta_{dc}\omega_{dc}\left(\nu_2\dot{U_{Low}} + \nu_3\dot{U_{Up}}\right) + \omega_{dc}^2\left(\lambda_2 U_{Low(t)} + \lambda_3 U_{Up(t)}\right) \end{bmatrix} \tag{20}$$

The dimensional parameters of the system are meticulously defined to facilitate normalized analysis and optimization. The mass ratio, denoted by μ, is defined as ($\mu \equiv \frac{m}{M}$), representing the ratio of the inerter mass \(m\) to the main mass M. The inerter ratios, β_1, β_2, and β_3, are defined for each respective inerter coefficient as ($\beta_i \equiv \frac{b_i}{M}$), where b_i are the inerter coefficients. Stiffness ratios are represented by λ_1, λ_2, λ_3, and Λ, defined by ($\lambda_i \equiv \frac{k_i}{K_1}$) for $(i = 1, 2, 3)$, and ($\Lambda \equiv \frac{K_2}{K_1}$), where k_i are the stiffness coefficients and K_1 and K_2 are the system stiffnesses. Similarly, damping ratios ν_1, ν_2, ν_3, and N are defined as ($\nu_i \equiv \frac{c_i}{C_1}$) and ($N \equiv \frac{C_2}{C_1}$), where c_i are the damping coefficients and C_1 and C_2 are the system damping coefficients. The decoupled natural frequency $\omega_{dc}$and the damping

ratio ζ_{dc} are defined using the lower base parameters as ($\omega_{dc} \equiv \sqrt{\frac{K_1}{M}}$) and ($\zeta_{dc} \equiv \frac{C_1}{2M\omega_{dc}}$), respectively. Additionally, the parameter $F_{(t)}^{'}$ is defined as $F_{(t)}^{'} \equiv \frac{F_{(t)}}{M}$, normalizing the external force by the main system mass. Lastly, the dimensional frequency Ω is defined as ($\Omega \equiv \frac{\omega}{\omega_{dc}}$), relating the excitation frequency ω to the decoupled system's natural frequency.

3.3. Semi-analytical Solutions for Harmonic and Synchronized Motion

The semi-analytical method involves proposing a solution for the generalized coordinate of the system, which has unknown coefficients but a known structure. The unknown coefficients are then determined by applying boundary and initial conditions. The analysis assumes that the bases and the harmonic excitation are in harmonic synchrony, meaning they all function at the same frequency of ω at the same time. Thus, the generalized coordinate system can be written as the steady-state response as:

$$q = \begin{bmatrix} U(t) \\ u(t) \end{bmatrix} = \begin{bmatrix} A \\ a \end{bmatrix} e^{j\omega t} \tag{21}$$

where ω is the excitation frequency and A and a are the vibration amplitudes of the main and DVA systems, respectively. Harmonic excitation of the main system's mass and the harmonic motion of the bases can be further characterized as:

$$F_{(t)}^{'} = f e^{j\omega t} \tag{22}$$

$$U_{Low(t)} = A_{Low} e^{j\omega t} \tag{23}$$

$$U_{Up(t)} = A_{Up} e^{j\omega t} \tag{24}$$

The amplitude of the main system's excitation is denoted by f, while A_{Low} and A_{Up} represent the amplitudes of the motion of the lower and upper bases, respectively. By replacing into the, the equation of motion of the system may be reformulated as:

$$\begin{bmatrix} A \\ a \end{bmatrix} = \omega_{dc}^2 \left((-\Omega^2[M] + 2j\omega\zeta_{dc}\Omega[C] + [K]) e^{j\omega t} \right)^{-1} [f] \tag{25}$$

3.4. System Parameters

In order to evaluate the introduced algorithm, a numerical analysis was carried out using arbitrary values for the main system, listed in Tab.1.

Table 1: Numerical Case Study Parameters

Main System Parameters	Value
Λ	1
N	1
$A_{Up} = A_{Low}$	0.0001
F	100
ω_{dc}	1000
ζ_{dc}	0.01

3.5. Decoupled Peak Slope Function

The dynamic behaviour of the system is encapsulated by the DPS functions, which aggregates the contributions of ten distinct sub-functions, each associated with specific system parameters:

$$DPS = \sum_{i=1}^{10} X_i(p_i) \tag{26}$$

where each $X_i(p_i)$ corresponds to parameters such as $\mu, \beta_1, \lambda_1, \nu_1, \beta_2, \lambda_2, \nu_2, \beta_3, \lambda_3$ and ν_3. The main system parameters are held constant and thus excluded from the DPS functions, as they represent fixed aspects of the actual system model.

Initial conditions for each sub-function are uniformly established:

$$X_i^{(0)} = X_{i,0}, \quad \forall i = 1, \dots, 10 \tag{27}$$

where $X_{i,0}$ denotes the initial value of each X_i at iteration $k = 0$. The parameters p_j associated with each sub-function are defined within specific ranges:

$$p_j \in \{p_{j,i},\ p_{j,i} + \Delta p_j, \dots, p_{j,f}\}, \quad \forall j = 1, \dots, 10. \tag{28}$$

Here, $p_{j,i}$ and $p_{j,f}$ represent the initial and final values of parameter p_j, respectively, with (Δp_j) indicating the incremental step size. The iterative procedure for updating each sub-function X_i is governed by the following equation:

$$X_{i(p_i)}^{(k+1)} = \mathrm{DPS}_{(p_i, \text{Other Parameters})} - \sum_{j \neq i}^{1} X_{j,(OtherParameters)} \ ; \begin{cases} p_i \in \{p_{i,i}, p_{i,i} + \Delta p_i, \dots, p_{i,f}\} \\ \text{for } i = 1,2, \dots, 10 \\ \text{for } k = 0,1, \dots \end{cases} \tag{29}$$

This equation updates each X_i based on the current DPS value and the sum of all other sub-functions from the previous iteration (k). The iterative process continues until convergence is achieved. Each $X_i(p_i)^{(k)}$ serves as a data point in the optimization framework. Approximate functions are employed to estimate the behaviour of each X_i across iterations, facilitating efficient and accurate optimization of the DPS function.

3.6. Performance of Polynomial Fits

The performance of various polynomial fitting methods was assessed to determine the most accurate approximation of the DPS sub-function. Fig. 3 and Table 2 summarize the results based on mean error, standard deviation, and RMSE. In each subplot of Figure 3, the x-axis shows the actual PS values, while the y-axis shows the corresponding estimations. Each point represents a unique DVA parameter set, with the red dashed line indicating a perfect fit. Accuracy improved with polynomial degree: the linear fit (Fig. 3a) showed the highest error ($RMSE = 1.4430 \times 10^{-10}$), followed by the quadratic fit (Fig. 3b), which reduced the RMSE to $8.3068 \times 10_{11}$. The cubic fit (Fig. 3c) achieved further improvement ($RMSE = 1.9874 \times 10^{11}$), while the quartic fit (Fig. 3d) yielded the best accuracy ($RMSE = 2.9908 \times 10_{-12}$), closely matching the perfect fit line. Thus, the quartic polynomial was selected as the optimal method for approximating the DPS function.

3.7. DPS Analysis Benchmark of a Fully Coupled 1DOF–1DOF System

A genetic algorithm (GA) was configured to benchmark the DPS method under identical design constraints. The GA used a population size of 150, evolved over 20 generations, with crossover and mutation probabilities of 0.70 and 0.20, respectively. All DVA variables were bounded between 0 and 1, except the mass ratio μ_1 , which was limited to [0, 0.75]. Each GA evaluation required a full frequency-response calculation, in contrast to the DPS method's closed-form surrogate evaluations. To assess the GA's stochastic performance, we executed one hundred independent runs with distinct random seeds. Despite occasional success in locating optimum PS values, the GA exhibited significant variability: the best PS across all runs was 4.3×10^{-5}, the mean PS was 4.4×10^{-5} and the worst PS reached 1.4×10^{-4}. By comparison, the DPS method deterministically achieved a PS of 6.9344×10^{-5} in a single pass. Table 3 contrasts the optimized parameter sets found by the DPS method with the GA's best, mean, and worst solutions. In terms of PS, the DPS optimum (6.9344×10^{-5}) lies between the GA's best (4.3×10^{-5}) and worst (1.4×10^{-4}), yet it is obtained without any randomness or repeated trials.

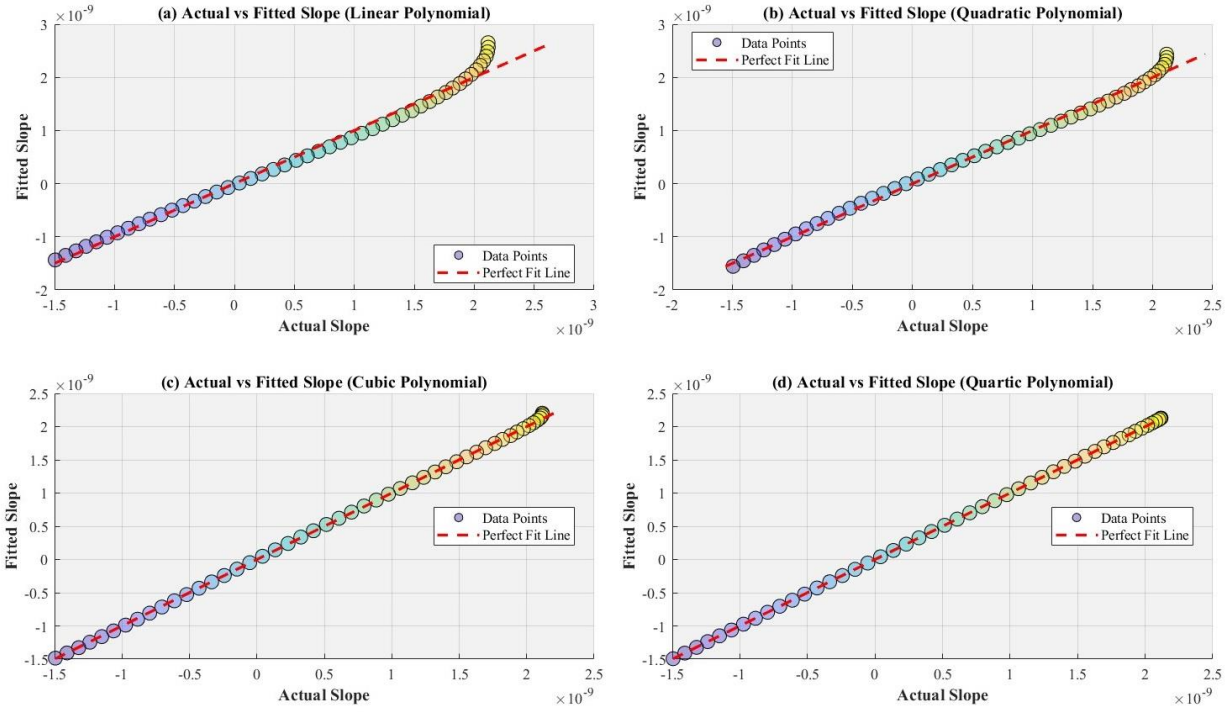

Figure 3: Polynomial fitting methods: (a) Linear, (b) Quadratic, (c) Cubic, (d) Quartic. Red dashed line: perfect fit; points: actual vs. predicted slopes.

Table 2: Polynomial Fit Methods Error Analysis

Fit Method	Mean Error	Standard Deviation	RMSE
Linear Polynomial	9.6730×10^{-11}	1.0819×10^{-10}	1.4430×10^{-10}
Quadratic Polynomial	5.8807×10^{-11}	5.9277×10^{-11}	8.3068×10^{-11}
Cubic Polynomial	1.2789×10^{-11}	1.5370×10^{-11}	1.9874×10^{-11}
Quartic Polynomial	1.5188×10^{-12}	2.6031×10^{-12}	2.9908×10^{-12}

Fig. 4 offers a visual comparison of FRFs generated by the proposed DPS method and three representative cases from 100 independent GA runs: the best, mean, and worst performers. The FRFs corresponding to the best and average GA outcomes display well-balanced resonance peaks and achieve slightly lower PS values than the DPS solution, confirming successful absorber tuning. However, the worst-case GA result reveals a clear mismatch between the peaks, demonstrating that the method can yield significantly suboptimal solutions. This comparison highlights a key limitation of GA-based optimization: its probabilistic nature leads to variability in solution quality and necessitates multiple runs to statistically find an optimal configuration. By contrast, the DPS method deterministically delivers a consistently high-quality solution in a single pass. Although its peak balancing may not always surpass the best GA run, its performance is reliably close and avoids the computational cost of repeated evaluations. These findings underscore the practical advantage of the DPS approach in applications where rapid computation, repeatability, and robustness are more critical than achieving a marginally lower PS value. This example also serves to clarify the functional effectiveness of the proposed method, reinforcing the mathematical narrative with visual and comparative evidence for broader reader accessibility.

Table 3. DPS versus GA parameter sets and PS metrics

	DPS optimum	Best GA	Mean GA	Worst GA
PS	6.9344×10^{-5}	4.3×10^{-5}	4.4×10^{-5}	1.4×10^{-4}
β^1	0.79	0.006	0.104	0.63
β^2	0.98	0.467	0.047	0.71

	DPS optimum	Best GA	Mean GA	Worst GA
β^3	0.47	0.338	0.422	0.31
λ^1	1.99	0.96	0.89	0.23
λ^2	0.83	0.62	0.57	0.72
λ^3	1.68	0.57	0.43	1
μ^1	0.17	0.49	0.05	0.4
ν^1	1.69	0.78	0.18	1
ν^2	1.49	0.13	0.54	0.97
ν^3	2.35	0.32	0.18	0.57

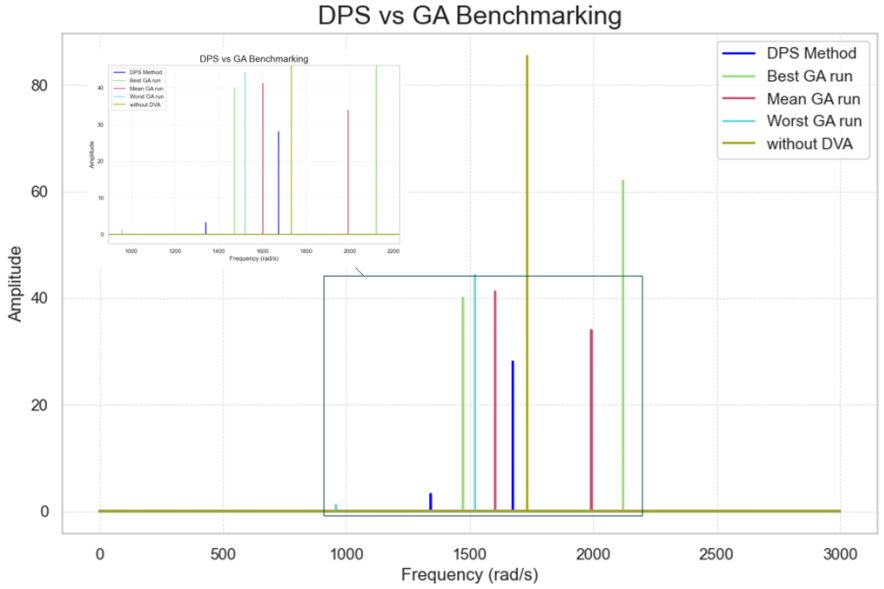

Figure 4. Comparison of frequency response functions (FRFs) between the DPS method and GA-based optimization for a benchmark system

3.8. Validation of the DPS procedure against the analytical solutions of lower degree systems

To assess the accuracy and robustness of the proposed DPS method, a validation study was conducted using a well-established lower-degree-of-freedom system for which analytical solutions are available. The core rationale is: if the decoupling procedure is valid, then the surrogate-based equations derived from a fully coupled system must yield correct results even when applied to a reduced-order model with fewer components. This ensures that the original coupling dynamics have been fully disentangled. To test this, the fully coupled 1DOF–1DOF system introduced earlier in the study served as the basis for surrogate construction. However, for validation, the DPS method was applied to a simplified benchmark system based on Asami et al.[34], where the main mass is connected to a fixed base via a spring and damper, and the DVA mass is linked to the main mass through another spring-damper pair (Fig.5).

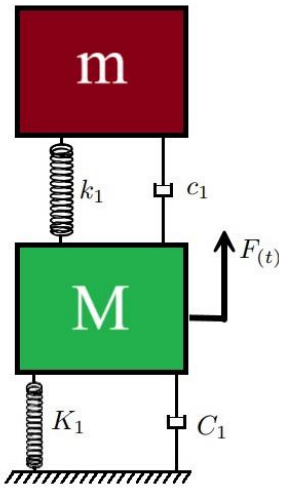

Figure 5: Schematic diagram of the system used for validation.

Asami et al.[34] derived both first-order and second-order analytical solutions for this setup. These were used to benchmark the DPS method, with structural parameters held constant: natural frequency $\Omega_{dc} = 14.14\Omega$, damping ratio $\zeta_{dc} = 0.24$, applied force of 100 N, and a mass ratio $\mu = 0.5$. The optimization objective was to determine the absorber stiffness ratio λ_1 and damping ratio ν_1 that minimize the Peak-Slope (PS) metric. The resulting optimized parameters and PS values are shown in Table 4.

Table 4. Comparison of Optimized Parameters and PS Metric for the Asami et al.[34] Benchmark System

Method	$\boldsymbol{\lambda_1}$	$\boldsymbol{\nu_1}$	PS Value
Asami (1st Order)	0.1525	4.568	0.59913
Asami (2nd Order)	0.1250	4.041	0.38587
DPS Method	0.1280	3.381	0.04915

Fig.6a presents the FRFs obtained using the Asami 1st-order formula, the Asami 2nd-order formula, and the proposed DPS method. All three methods yield similar overall system responses, validating the general accuracy of the DPS framework. However, a more detailed comparison is provided in Figure 6b, which displays a bar chart of the corresponding PS values. Here, the DPS method achieves a PS value that is nearly an order of magnitude smaller than those from both analytical approaches, indicating superior peak balancing and absorber tuning. This outcome confirms that the decoupling assumption embedded in the DPS framework holds even in simple, low-degree-of-freedom systems where analytical baselines are available. The implication is that if such accuracy is maintained at low DOFs, the method is likely to scale effectively to more complex systems with higher DOFs. Crucially, because the DPS optimization relies on minimizing the sum of precomputed surrogate functions, each representing a single absorber parameter, the computational burden is significantly reduced. This transforms the traditionally intensive DVA tuning process into a structured, repeatable, and low-cost procedure. By enabling direct use of these surrogate functions across varying system architectures, the method supports the development of reusable design catalogues. These catalogues eliminate the need for re-running time-consuming numerical optimizations, providing engineers with rapid access to near-optimal absorber configurations tailored to specific structural dynamics.

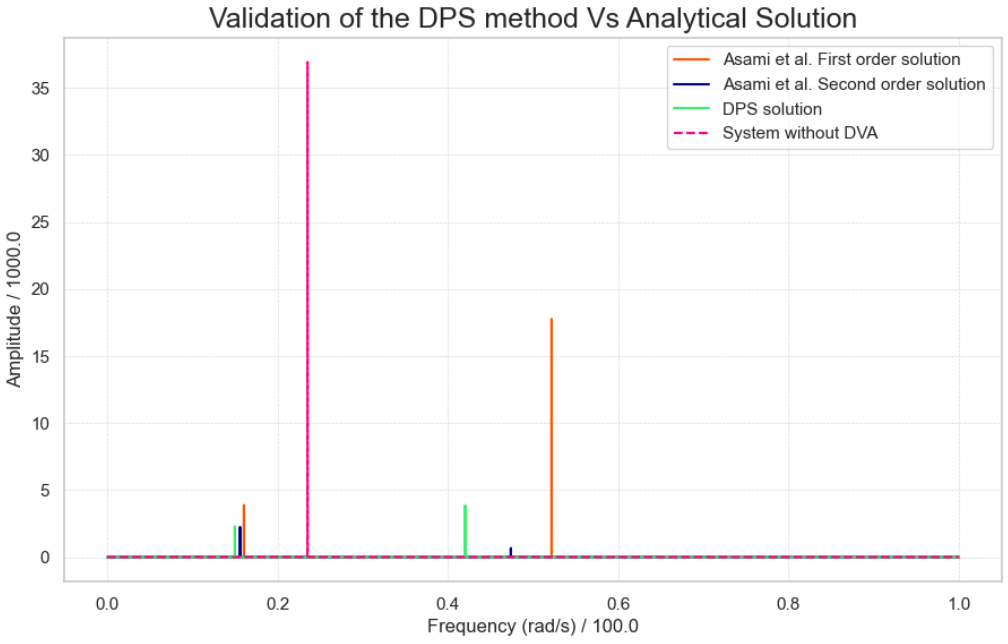

(a)

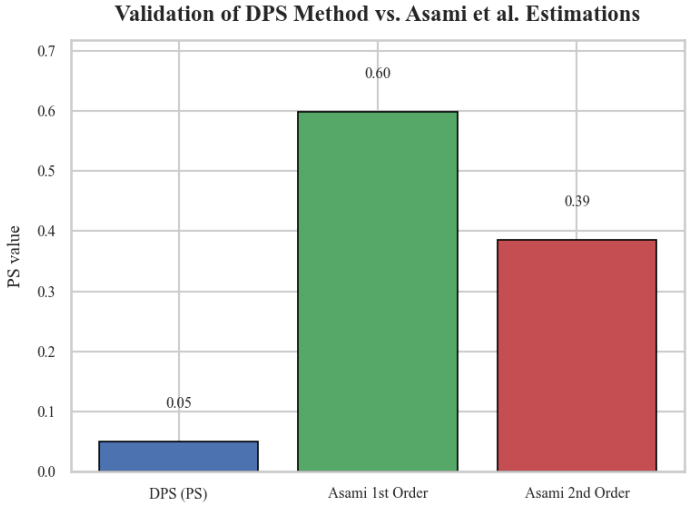

(b)

Figure 6: (a) Frequency response functions (FRFs) and (b) corresponding Peak-Slope (PS) values for the DPS method compared to Asami's first- and second-order analytical solutions.

4. Generalized Optimization Using Catalogues Derived from the DPS Framework

Following the successful validation of the DPS method, this section introduces a structured algorithm for creating design catalogues that enable rapid optimization of DVA parameters for a wide range of mechanical systems, even those that represent simplified subsystems of a fully coupled baseline model. The core principle of the DPS framework lies in its decoupling of the optimization space: each DVA parameter is isolated into its own univariate surrogate function derived from the original, fully coupled system. Importantly, this approach allows the resulting decoupled equations to be universally applied to any system configuration that falls within the modelled parameter ranges,

regardless of whether all elements of the full system are present.

This generality is made possible by the logic of the decoupling algorithm: if a system of interest lacks certain components from the full model (e.g., no inerter or a fixed damping value), the associated parameters are simply set to zero (if absent) or treated as constants (if fixed). However, even when a parameter is set to zero, its corresponding decoupled surrogate function must still be evaluated and included in the optimization process. This ensures that any residual influence from the full system model is properly accounted for in the reduced configuration.

The optimization objective is defined as minimizing the summation of all decoupled surrogate functions, regardless of whether the associated parameter is present in the system or not. In this formulation, the optimal set of DVA parameters is obtained when the total sum of all DPS functions approaches zero, indicating minimal peak variation and thus optimal vibration mitigation.

$$\text{Optimization Goal} \equiv \min \sum_{i=1}^{n} X_i(P_i) \tag{30}$$

where n is the total number of decoupled functions derived from the full system (including inactive or zero-valued parameters).

To support this algorithmic approach, a design catalogue was constructed from four distinct structural configurations of the fully coupled 1DOF–1DOF system, each characterized by a unique set of fixed structural properties (e.g., natural frequency, damping ratio, and mass ratios). For each configuration, ten decoupled surrogate functions were generated, each corresponding to a discrete variation of a single DVA parameter. These surrogate functions are represented as quartic polynomials:

$$X_i(p_i) = a_{i,0} + a_{i,1}p_i + a_{i,2}{p_i}^2 + a_{i,3}{p_i}^3 + a_{i,4}{p_i}^4 \tag{31}$$

The corresponding polynomial coefficients, along with the structural parameters for each case, are detailed in Table 5.

To use the catalogue for a given system:

1. **Identify available parameters**: Determine which DVA parameters exist in the system. Set any absent parameters to zero.
2. **Assign fixed values**: If some parameters are fixed due to design or physical constraints, substitute them accordingly.
3. **Set the available ranges for the DVA parameters**: For each parameter, retrieve the corresponding coefficient from the catalogue and create the surrogate functions.
4. **Perform optimization**: Minimize the sum of all DPS functions ($X_i(p_i)$) values (including those for zero or fixed parameters) over the range of free variables.
5. **Extract the set of optimum DVA values**: The set of DVA values that minimizes the summation of the DPS values ($\min \sum_{i=1}^{n} X_i(P_i)$) is the optimum DVA value set.

This formulation enables the rapid identification of **near-optimal DVA designs** for any subsystem related to the original fully coupled model. Because the catalogue captures a comprehensive mapping of parameter influence on vibration suppression, it allows for efficient reuse across diverse applications, eliminating the need for re-running high-fidelity simulations.

Table 5a. Structural parameters for the four benchmark systems

System	Λ	N	$A_{Up} = A_{Low}$	F	ω_{dc}	ζ_{dc}
1	1.00	1.00	1×10^{-4}	100	1000	0.01
2	0.75	0.75	1×10^{-4}	100	800	0.02
3	0.50	0.50	1×10^{-4}	100	800	0.02
4	0.50	0.50	1×10^{-4}	100	700	0.03

Table 5b. Quartic coefficients of the DPS model for 4 distinct systems

System 1					
Coefficients	a_4	a_3	a_2	a_1	a_0
μ_1	−8.2269e−12	2.2743e−10	−2.1919e−09	8.5432e−09	−1.1436e−08
β_1	1.2785e−11	−2.9913e−10	2.6576e−09	−8.3011e−09	−2.7080e−09
λ_1	3.3333e−12	−1.1461e−10	6.9518e−10	−2.7359e−10	1.1169e−09
ν_1	3.4793e−12	−7.5003e−11	5.1341e−10	−2.7621e−09	1.5231e−08
β_7	4.3369e−11	−9.1300e−10	5.6815e−09	−1.1223e−08	2.5909e−08
λ_7	−4.6563e−11	9.9032e−10	−6.4370e−09	1.3672e−08	−2.7614e−08
ν_7	−3.1186e−12	8.3988e−11	−5.1866e−10	9.5108e−10	−1.3858e−10
β_8	−3.0277e−11	1.1787e−09	−1.5057e−08	6.9366e−08	−6.3326e−08
λ_8	2.4785e−11	−1.0481e−09	1.3963e−08	−6.5790e−08	6.0165e−08
ν_8	1.7830e−13	−2.1887e−11	5.8945e−10	−4.1231e−09	4.9205e−09
System 2					
Coefficients	a_4	a_3	a_2	a_1	a_0
μ_1	−4.2169e−12	1.2141e−10	−1.2323e−09	5.5550e−09	−1.1764e−08
β_1	1.0636e−11	−2.3902e−10	1.9574e−09	−5.1823e−09	−2.0384e−09
λ_1	4.8080e−13	−4.7496e−11	2.8672e−10	6.2064e−11	−5.8066e−10
ν_1	1.3318e−13	1.4513e−11	−3.3418e−10	4.6261e−10	1.1578e−08
β_7	6.1234e−11	−1.2616e−09	7.7004e−09	−1.4060e−08	2.3311e−08
λ_7	−6.3736e−11	1.3240e−09	−8.3711e−09	1.6329e−08	−2.4919e−08
ν_7	−3.4698e−12	9.3584e−11	−5.9060e−10	1.1988e−09	−3.8190e−10
β_8	1.4112e−12	4.8618e−10	−1.0332e−08	6.0675e−08	−7.2392e−08
λ_8	−3.6533e−12	−4.3901e−10	9.9743e−09	−5.9718e−08	7.2568e−08
ν_8	8.7218e−13	−4.2572e−11	8.3451e−10	−5.3544e−09	6.7529e−09
System 3					
Coefficients	a_4	a_3	a_2	a_1	a_0
μ_1	−4.1081e−12	1.1424e−10	−1.1141e−09	4.9374e−09	−1.1596e−08
β_1	1.2882e−11	−2.8725e−10	2.1328e−09	−4.1703e−09	−3.1410e−09
λ_1	−1.3282e−12	8.7284e−12	−2.0724e−10	1.2659e−09	−2.3467e−09
ν_1	−3.0662e−13	2.7309e−11	−4.3590e−10	4.8020e−10	1.3097e−08
β_7	5.5906e−11	−1.0275e−09	4.6508e−09	−2.4566e−10	9.8006e−09
λ_7	−5.9476e−11	1.1141e−09	−5.5237e−09	3.0669e−09	−1.1962e−08
ν_7	−3.7642e−12	9.6193e−11	−5.2460e−10	6.3498e−10	5.4645e−10
β_8	−2.6076e−11	1.3459e−09	−1.9714e−08	1.0138e−07	−1.2572e−07
λ_8	2.4964e−11	−1.3287e−09	1.9607e−08	−1.0115e−07	1.2625e−07
ν_8	8.9637e−13	−5.0816e−11	1.0127e−09	−6.3609e−09	7.4244e−09
System 4					
Coefficients	a_4	a_3	a_2	a_1	a_0
μ_1	1.0580e−11	−3.3315e−10	3.8848e−09	−1.9060e−08	2.9010e−08
β_1	6.9658e−12	−1.2374e−10	5.0191e−10	2.2950e−09	−9.1548e−09
λ_1	−1.1743e−11	3.0699e−10	−3.3189e−09	1.5790e−08	−3.0429e−08
ν_1	2.4462e−12	−5.2918e−11	4.2835e−10	−3.7223e−09	2.1408e−08
β_7	−2.4987e−11	6.6586e−10	−4.7916e−09	−4.3244e−09	1.0973e−07
λ_7	8.3603e−13	7.0632e−11	−3.6724e−09	4.5886e−08	−1.8443e−07
ν_7	−2.6664e−12	6.3649e−11	−1.6792e−10	−1.0670e−09	3.5905e−09
β_8	4.9277e−11	−1.9031e−09	2.8576e−08	−1.9746e−07	5.2849e−07
λ_8	−4.0292e−11	1.6182e−09	−2.5352e−08	1.8158e−07	−4.9873e−07

ν_8	9.2586e−12	−3.0220e−10	3.8118e−09	−2.0104e−08	3.2698e−08

As an example, the frequency response function (FRF) of System 1, optimized using the DPS method across different parameter ranges, is presented in Fig 7.

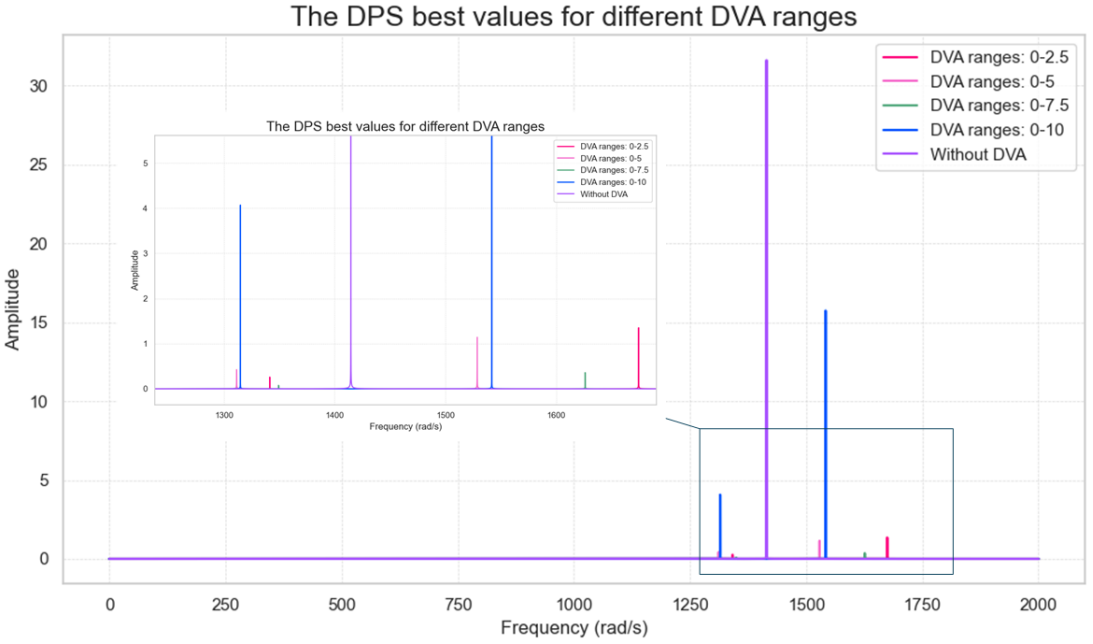

Figure 7. Frequency response functions (FRFs) of System 1 optimized using the DPS method across various parameter ranges.

The variation of surrogate coefficients with changes in structural parameters has not been explored in this study. A general catalogue that accounts for both structural and absorber variability would require an expanded parameter space, new sampling methods, and potentially alternative surrogate models. This direction was intentionally excluded in order to maintain clarity of scope and focus on validating absorber-only decoupling against full genetic algorithms. To partially address this limitation, a sensitivity analysis has been included in Appendix A, where structural parameters are varied while absorber values are held fixed. The relative error between the surrogate-based DPS and the full-model PS is recorded across a realistic parameter range. Strong agreement is observed, suggesting that the surrogate model remains accurate under moderate structural variation. This provides support for the current formulation and motivates future work toward more generalized, structure-inclusive surrogate frameworks.

5. Conclusion

This study presents a novel and computationally efficient surrogate-assisted optimization framework for tuning dynamic vibration absorbers (DVAs), specifically designed to address the high computational demands of traditional methods in complex mechanical systems. At the core of this framework is the introduction of the Peak-Slope (PS) metric, a generalization of the classical equal-peak tuning criterion, which quantifies absorber effectiveness by measuring the secant slope between adjacent resonance peaks. Optimal tuning corresponds to the configuration that minimizes this slope, offering a direct and physically interpretable measure of vibration mitigation. A key innovation of the framework is the decoupling of the parameter space into independent subspaces (structural, absorber, and excitation), which enables targeted surrogate modeling using quartic polynomial regression. These surrogate models replace full analytical evaluations within a genetic algorithm (GA) optimization loop, reducing computation times from hours to seconds without compromising accuracy. To validate the generality and accuracy of the proposed approach, a benchmark fully coupled 1DOF–1DOF system with further comparison against analytical solutions from reduced-order models is employed. The results demonstrate not only excellent agreement with established methods but, in some cases, superior performance of the proposed Decoupled Peak-Slope (DPS) approach in minimizing resonance responses. This confirms that the decoupling strategy preserves the essential system dynamics while enabling flexible and efficient optimization across diverse configurations. Building on this, the study introduces a

catalogue of precomputed surrogate models—quartic polynomial representations of the PS metric across various structural configurations and parameter ranges. This database allows for rapid evaluation and optimization of DVA settings, even for partially defined or simplified systems. The surrogate catalogue thus transforms from a computational shortcut into a practical design tool that supports near-instantaneous DVA tuning for real-world applications. One of the most promising directions for future research lies in extending this framework to semi-active DVA systems, where absorber parameters can be dynamically adjusted in real time—such as through magnetorheological dampers or variable stiffness mechanisms. In such cases, rapid recalibration of absorber properties is often required in response to changes in external excitation or structural conditions. The use of precomputed, decoupled surrogate equations enables real-time, non-iterative optimization, bypassing the need for repeated simulations or GA runs. By minimizing the sum of relevant surrogate functions for a given state, optimal absorber settings can be directly inferred, allowing on-the-fly tuning. This lays the groundwork for both improved passive solutions and advanced real-time control in semi-active systems, particularly in fields such as aerospace, automotive engineering, and adaptive civil infrastructure.

In addition, a new research direction aims to extend the current framework beyond a fixed structural configuration. As implemented, the decoupling method assumes a static host structure, with the surrogate catalogue tailored to a specific set of system parameters. However, preliminary results from the sensitivity analysis presented in **Appendix A** suggest that the DPS formulation retains strong predictive performance even under moderate variations in structural parameters. This finding motivates the exploration of a more generalized surrogate architecture, potentially a *meta-catalogue*, that encodes not only DVA dynamics but also correlations between structural and absorber parameters. Such an approach would support the rapid generation of DPS surrogates across diverse structural configurations, thereby significantly enhancing the framework's modularity and adaptability. Realizing this capability would require the development of new methods for cross-domain sampling, parametric encoding of structural features, and hierarchical surrogate modelling. Nonetheless, if successful, it could enable a unified and transferable DVA optimization engine suitable for adaptive or time-varying hosts.

In conclusion, this study provides a foundational advancement toward the development of a modular, scalable, and adaptable framework for the optimization of dynamic vibration absorbers (DVAs). By enabling efficient surrogate-assisted tuning across a wide range of configurations, the proposed approach not only supports improved passive vibration mitigation but also paves the way for real-time control in semi-active systems. Furthermore, the generality and flexibility of the decoupled surrogate modelling strategy suggest promising potential for broader application in structurally diverse environment that this lays the groundwork for future development of universally applicable tuning methodologies.

Appendix A: Sensitivity Analysis of the structural parameters of the system for the fixed values of the DVA parameters

To perform a sensitivity analysis, the effect of variations in the main system parameters is investigated while the DVA parameters are held fixed. This approach is intended to provide insight into how changes in the main system parameters influence the DPS. Although the method is highly preliminary, it is considered worthwhile, as it offers valuable understanding of the DPS's dependency on the main system parameters under constant DVA configurations. The analysis is carried out by evaluating how the main system parameters vary across different fixed sets of dimensional DVA parameters, and how these variations affect the DPS, which is initially influenced by all parameters. The relative error, used as the primary performance metric, is defined as the error between the DPS approximation and the actual PS obtained from the fully coupled system 1 model which is derived by the fixed values of the main system and the variation of the DVA parameters.

- An extensive analysis of the main system parameters should be conducted, covering a wide range for each parameter within the predefined boundary. This step is essential as it offers a comprehensive perspective on how the main system parameters impact on the DPS across a broad spectrum of DVA parameter values.
- Variety in DVA parameter values: The study includes changing DVA parameters within a predetermined range (e.g., 0 to 1) to examine the impact of different DVA parameter values on the pre calculated DPS.

The following figures show the sensitivity of different parameters for different variations of the DVA parameters,

respectively.

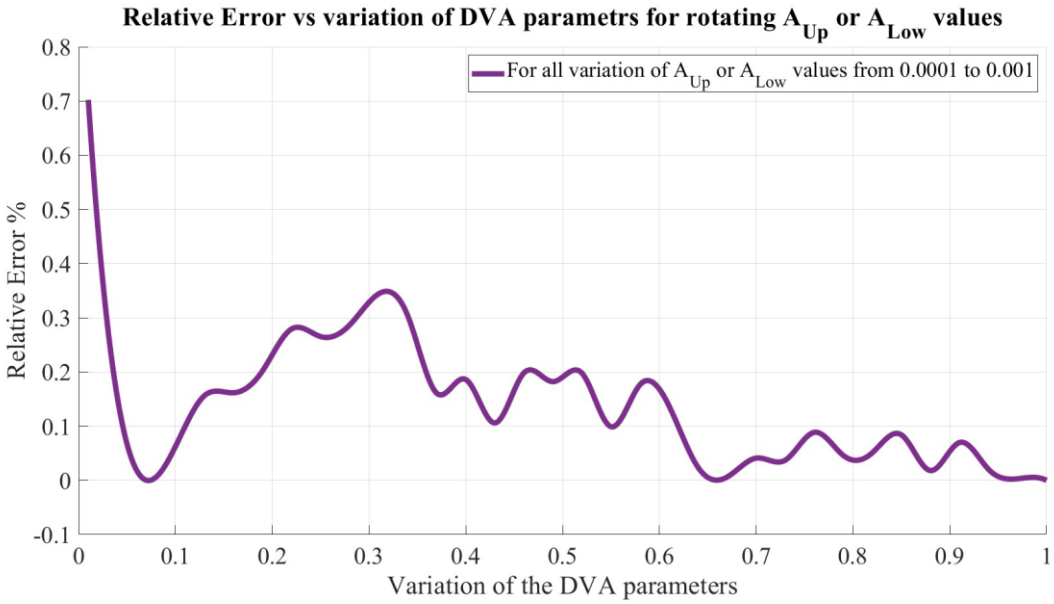

Figure A.1: Sensitivity analysis of A_{Low} and A_{Up} for different variation of the DVA parameters

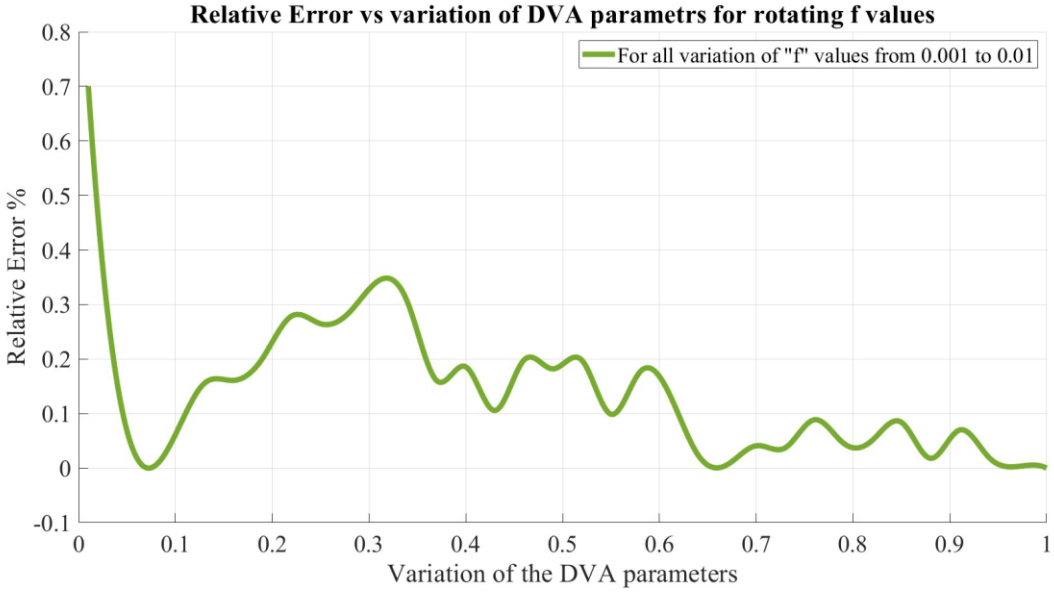

Figure A.2: Sensitivity analysis of F for different variation of the DVA parameters

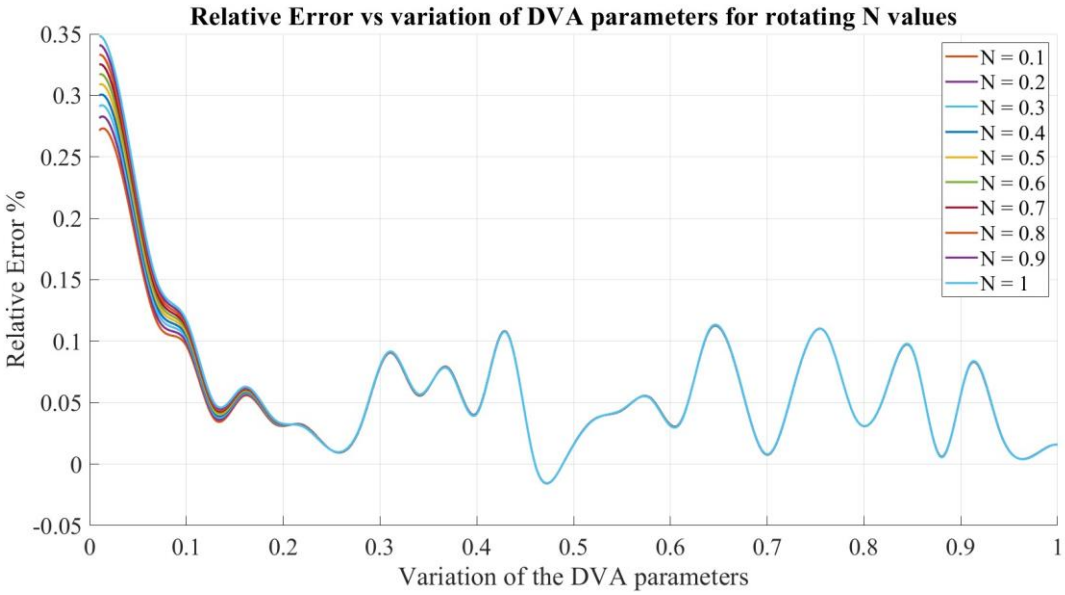

Figure A.3: Sensitivity analysis of the N for different variation of the DVA parameters

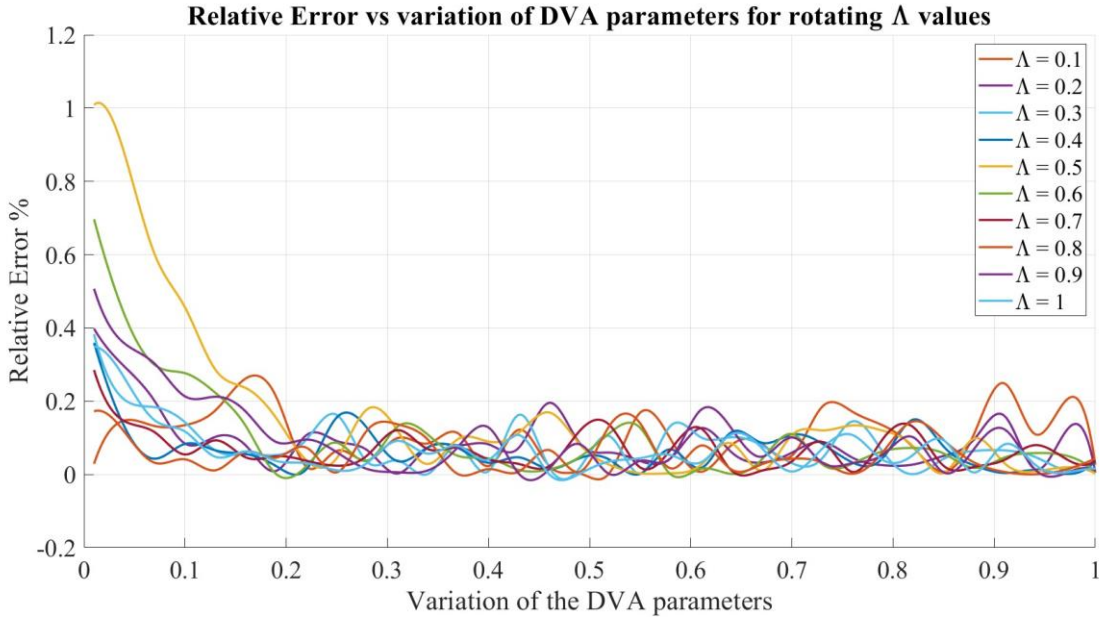

Figure A.4: Sensitivity analysis of the Λ for different variation of the DVA parameters

The results of the sensitivity analysis provide important validation for the robustness of the DPS formulation. By systematically varying key structural parameters while keeping the DVA parameters fixed, it is shown that the relative error between the DPS prediction and the PS response remained consistently low. In most cases, the relative error stayed below 1%, with typical values well under 0.5%, indicating that the decoupled surrogate retains a high degree of accuracy even when applied to structural configurations that deviate moderately from the original training case. Notably, even parameters that significantly alter the system's modal characteristics, such as ω_{dc} and ζ_{dc}, produced minimal degradation in DPS performance across the tested range. These findings reinforce the idea that, within practical bounds, the DPS surrogate behaves largely independently of the host structure, thereby validating its use in modular and reusable absorber design workflows.

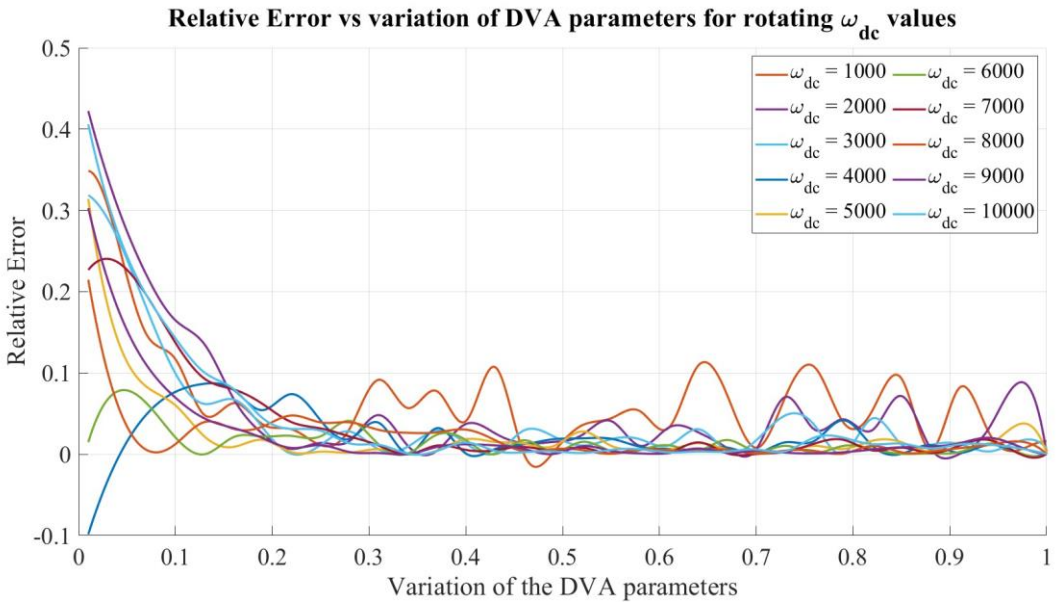

Figure A.5: Sensitivity analysis of the ω_{dc} for different variation of the DVA parameters

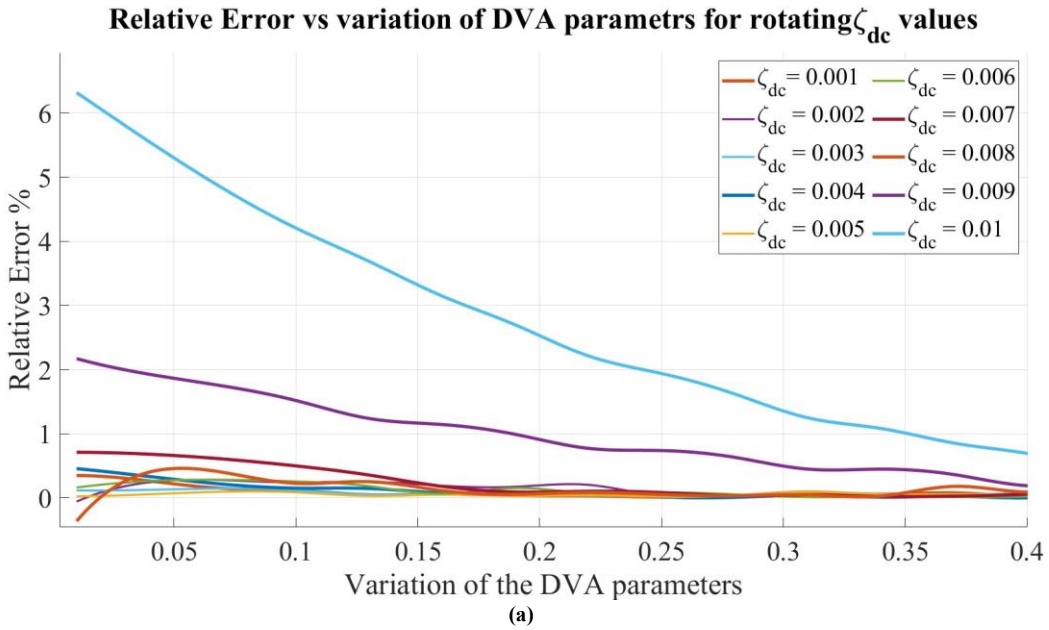

(a)

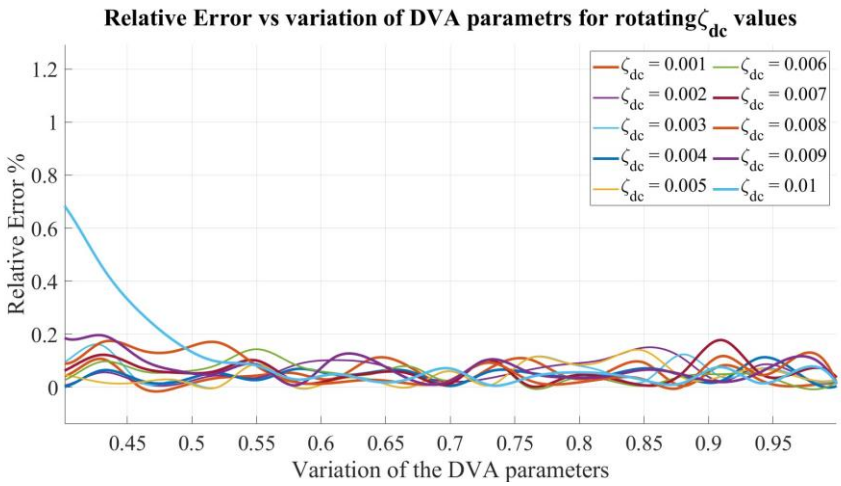

(b)

Figure A.6: Sensitivity analysis of the zeta_{dc} for different variations of the DVA parameters (a) ranges from 0 to 0.4, and (b) ranges from 0.4 to 1.

Acknowledgments

The author would like to thank the reviewers for constructive valuable and criticisms comments, also, they are thankful to the Iranian Nanotechnology Development Committee for their financial support and the University of Kashan for supporting this work by Grant No. 1311761/4.

References

[1] Z. Liu, K. Zhou, L. Wang, T. Jiang, H. Dai, Dynamical stability of cantilevered pipe conveying fluid in the presence of linear dynamic vibration absorber, *Journal of Computational Applied Mechanics,* Vol. 50, No. 1, pp. 182-190, 2019.

[2] F. Freddi, C. Galasso, G. Cremen, A. Dall'Asta, L. Di Sarno, A. Giaralis, F. Gutiérrez-Urzúa, C. Málaga-Chuquitaype, S. A. Mitoulis, C. Petrone, Innovations in earthquake risk reduction for resilience: Recent advances and challenges, *International Journal of Disaster Risk Reduction,* Vol. 60, pp. 102267, 2021.

[3] T. E. Saaed, G. Nikolakopoulos, J.-E. Jonasson, H. Hedlund, A state-of-the-art review of structural control systems, *Journal of Vibration and Control,* Vol. 21, No. 5, pp. 919-937, 2015.

[4] X. Song, J. Liu, M. Xia, Advanced Vibration-Based Fault Diagnosis and Vibration Control Methods, 18, MDPI, 2023, pp. 7704.

[5] M. Jafari, M. Mohammadimehr, Forced vibration control of Timoshenko's micro sandwich beam with CNT/GPL/CNR reinforced composites integrated by piezoelectric on Kerr's elastic foundation using MCST, *Journal of Computational Applied Mechanics,* Vol. 56, No. 1, pp. 15-42, 2025.

[6] A. M. Zenkour, H. D. El-Shahrany, Forced vibration of a magnetoelastic laminated composite beam on Pasternak's foundation, *Journal of Computational Applied Mechanics,* Vol. 52, No. 3, pp. 478-497, 2021.

[7] H. Frahm, Device for damping vibrations of bodies, 1911.

[8] J. Ormondroyd, J. P. Den Hartog, The theory of the dynamic vibration absorber, *Journal of Fluids Engineering,* Vol. 49, No. 2, 1928.

[9] J. P. Den Hartog, 1985, *Mechanical vibrations*, Courier Corporation,

[10] R. E. D. Bishop, D. B. Welbourn, The problem of the dynamic vibration absorber, *Engineering, London,* Vol. 174, pp. 769, 1952.

[11] J. E. Brock, A note on the damped vibration absorber, 1946.

[12] W.-H. L. M. R. Roohollah Talebitooti, Concurrent energy harvesting and vibration suppression utilizing PZT-based dynamic vibration absorber, *Archive of Applied Mechanics*, pp. 1-20, 2022.

[13] S. Mehdi Mohammadimehr Saeid, Vibration analysis of rotating fully-bonded and delaminated sandwich beam with CNTRC face sheets and AL-foam flexible core in thermal and moisture environments, *Mechanics Based Design of Structures and Machines,* Vol. 48, No. 5, pp. 584-614, 2020.

[14] F. L. M. B. M. V. S. M. Antonio Argentino, SMA-based adaptive tuned mass dampers: Analysis and comparison, *Mechanical Systems and Signal Processing,* Vol. 186, pp. 109883, 2023.

[15] N. Duy Chinh, Vibration control of a rotating shaft by passive mass-spring-disc dynamic vibration absorber, *Archive of Mechanical Engineering,* Vol. 67, No. 3, pp. 279-297, 2020.

[16] M. M. M. Mohammadimehr, Stability and free vibration analyses of double-bonded micro composite sandwich cylindrical shells conveying fluid flow, *Applied Mathematical Modelling,* Vol. 47, pp. 685-709, 2017.

[17] B. R. N. M. M. S Javad Atifeh, Stress and free vibration analysis of piezoelectric hollow circular FG-SWBNNTs reinforced nanocomposite plate based on modified couple stress theory subjected to thermo-mechanical loadings, *Journal of Vibration and Control,* Vol. 24, No. 15, pp. 3471-3486, 2018.

[18] R. R. M. Mohammadimehr, Bending and vibration analyses of a rotating sandwich cylindrical shell considering nanocomposite core and piezoelectric layers subjected to thermal and magnetic fields, *Applied Mathematics and Mechanics,* Vol. 39, No. 2, pp. 219-240, 2018.

[19] M. M. A. A. Monajemi, Stability analysis of a spinning soft-core sandwich beam with CNTs reinforced metal matrix nanocomposite skins subjected to residual stress, *Mechanics Based Design of Structures and Machines,* Vol. 52, No. 1, pp. 338-358, 2024.

[20] S.-B. Choi, Y.-M. Han, 2016, *Piezoelectric actuators: control applications of smart materials*, CRC Press,

[21] Z. Deng, M. J. Dapino, Review of magnetostrictive materials for structural vibration control, *Smart Materials and Structures,* Vol. 27, No. 11, pp. 113001, 2018.

[22] M. S. K. Jacob, Damping of Smart Systems by Shape Memory Alloys (SMAs).

[23] M. Arabzadeh-Ziari, M. Mohammadimehr, E. Arabzadeh-Ziari, M. Asgari, Deflection, buckling and vibration analyses for a sandwich nanocomposite structure with foam core reinforced with GPLs and SMAs based on TSDBT, *Journal of Computational Applied Mechanics,* Vol. 55, No. 2, pp. 289-321, 2024.

[24] Z. K. Maraghi, S. A. Mirhaj, Ö. Civalek, Instability and vibration behaviour of sandwich plate on Kerr foundation, *Engineering Structures,* Vol. 341, pp. 120876, 2025.

[25] M. A. Mohammadimehr, A. Loghman, S. Amir, M. Mohammadimehr, E. Arshid, Ö. Civalek, Magneto-electro vibration analysis of a moderately thick double-curved sandwich panel with porous core and GPLRC using FSDT, *Journal of Computational Applied Mechanics,* Vol. 56, No. 3, pp. 673-693, 2025.

[26] F. Ghasemi, A. Salari, E. Salari, A. Rastgoo, Machine learning-assisted investigation on nonlinear vibration analysis of bio-inspired auxetic tubes, *International Journal of Structural Integrity*, 2025.

[27] H. Ezzati, S. Pashalou, A. Rastgoo, F. Ebrahimi, Vibration analysis of multilayer graphene origami-enabled metamaterial plates, *Acta Mechanica,* Vol. 235, No. 12, pp. 7623-7640, 2024.

[28] E. Haghparast, A. G. Arani, A. H. S. Arani, Vibration of axially moving sandwich plate with honeycomb core and nanocomposite face sheets, *Steel and Composite Structures,* Vol. 55, No. 5, pp. 433, 2025.

[29] S. Givi, A. Ghorbanpour Arani, Z. Khoddami Maraghi, E. Arshid, Free vibration and supersonic flutter analyses of a sandwich cylindrical shell with CNT-reinforced honeycomb core integrated with piezoelectric layers, *Mechanics Based Design of Structures and Machines,* Vol. 53, No. 5, pp. 3225-3253, 2025.

[30] W. J. Carter, F. C. Liu, Steady-state behavior of nonlinear dynamic vibration absorber, 1961.

[31] A. G. Thompson, Optimum tuning and damping of a dynamic vibration absorber applied to a force excited and damped primary system, *Journal of Sound and Vibration,* Vol. 77, No. 3, pp. 403-415, 1981.

[32] O. Nishihara, T. Asami, Closed-form solutions to the exact optimizations of dynamic vibration absorbers (minimizations of the maximum amplitude magnification factors), *J. Vib. Acoust.,* Vol. 124, No. 4, pp. 576-582, 2002.

[33] T. Asami, O. Nishihara, H 2 optimization of the three-element type dynamic vibration absorbers, *J. Vib. Acoust.,* Vol. 124, No. 4, pp. 583-592, 2002.

[34] T. Asami, O. Nishihara, A. M. Baz, Analytical solutions to H∞ and H 2 optimization of dynamic vibration absorbers attached to damped linear systems, *J. Vib. Acoust.,* Vol. 124, No. 2, pp. 284-295, 2002.

[35] H. Yamaguchi, Damping of transient vibration by a dynamic absorber, *Trans. Jpn. Soc. Mech. Eng.,* Vol. 54, No. 499, pp. 561, 1988.

[36] O. Nishihara, H. Matsuhisa, others, Design of a dynamic vibration absorber for minimization of maximum amplitude magnification factor (derivation of algebraic exact solution), *Japanese Society of Mechanical Engineering,* Vol. 63, pp. 3438-3445, 1997.

[37] F. Sadek, B. Mohraz, A. W. Taylor, R. M. Chung, A method of estimating the parameters of tuned mass dampers for seismic applications, *Earthquake Engineering \& Structural Dynamics,* Vol. 26, No. 6, pp. 617-635, 1997.

[38] H.-C. Tsai, G.-C. Lin, Optimum tuned-mass dampers for minimizing steady-state response of support-excited and damped systems, *Earthquake engineering \& structural dynamics,* Vol. 22, No. 11, pp. 957-973, 1993.

[39] J. H. Ruoyu Zhang, Hybrid Analytical Optimal Approach and Comparative Analyses for Tuned Viscous Mass Damper with Negative Stiffness (TVMDNS), *Journal of Vibration Engineering \& Technologies*, pp. 1-18, 2024.

[40] T. Igusa, K. Xu, Vibration control using multiple tuned mass dampers, *Journal of sound and vibration,* Vol. 175, No. 4, pp. 491-503, 1994.

[41] A. J. Clark, others, Multiple passive tuned mass dampers for reducing earthquake induced building motion, in *Proceeding of,* 779-784.

[42] H. Anthony Frederick, *Multi-degree of freedom passive and active vibration absorbers for the control of structural vibration*, Thesis, 2003.

[43] J. C. S. J. J. Yong, Geometrical design method of multi-degree-of-freedom dynamic vibration absorbers, *Journal of Sound and Vibration,* Vol. 303, No. 1-2, pp. 343-356, 2007.

[44] D. G. T. Y. Q. W. Y. S. Jinsong Zhou, Multi-degree of Freedom Dynamic Vibration Absorber of the Carbody of High-Speed Trains, in *Proceeding of,* 3-7.

[45] D. G. Y. J. Y. S. Jinsong Zhou, Study on multi-degree of freedom dynamic vibration absorber of the car body of high-speed trains, *Mechanical Sciences,* Vol. 13, No. 1, pp. 239-256, 2022.

[46] R. B. B. A. K. W. A. K. S. Rj Alkhoury, *Ride dynamic analysis of a hybrid discrete and continuous vehicle model*, pp. 2008.

[47] F. Mariano, Optimal parameters and characteristics of a three degree of freedom dynamic vibration absorber, 2012.

[48] S.-P. Y. G.-S. G. Y.-J. S. Lin Wang, Nonlinear dynamical analysis and parameters optimization of four semi-active on-off dynamic vibration absorbers, *Journal of Vibration and Control,* Vol. 19, No. 1, pp. 143-160, 2013.

[49] T. Szolc, Medium frequency dynamic investigation of the railway wheelset-track system using a discrete-continuous model, *Archive of Applied Mechanics,* Vol. 68, pp. 30-45, 1998.

[50] A. F. B. Noori, Optimum design of dynamic vibration absorbers for a beam, based on H∞ and H 2 Optimization, *Archive of Applied Mechanics,* Vol. 83, pp. 1773-1787, 2013.

[51] W. Chia-Man Chang Yi-Ren, Elastic beam with nonlinear suspension and a dynamic vibration absorber at the free end, *Transactions of the Canadian Society for Mechanical Engineering,* Vol. 38, No. 1, pp. 107-137, 2014.

[52] H. D. H. P. P Frank Pai, Acoustic multi-stopband metamaterial plates design for broadband elastic wave absorption and vibration suppression, *International journal of mechanical sciences,* Vol. 103, pp. 104-114, 2015.

[53] C. Tianxing Wu Rong, Vibration control of base system using distributed dynamic vibration absorbers, *Journal of Vibration and Control,* Vol. 20, No. 10, pp. 1589-1600, 2014.

[54] L. C. C. Y. Deyu Li, Dynamic vibration absorbers for vibration control within a frequency band, *Journal of Sound and Vibration,* Vol. 330, No. 8, pp. 1582-1598, 2011.

[55] C. A. C. C. Gregorio Toscano Pulido, Multiobjective structural optimization using a microgenetic algorithm, *Structural and Multidisciplinary Optimization,* Vol. 30, pp. 388-403, 2005.

[56] A. C. G. L. J. H. G. Z. Zheng-Dong Ma, Design optimization of a runflat structure based on multi-objective genetic algorithm, *Structural and Multidisciplinary Optimization,* Vol. 51, pp. 1363-1371, 2015.

[57] Y. X. J. B. N. S. Zhaoqing Chen, Hybrid analytical H-norm optimization approach for dynamic vibration absorbers, *International Journal of Mechanical Sciences,* Vol. 264, pp. 108796, 2024.

[58] R. Gaetan Kerschen Ghislain, H_∞ optimization of multiple tuned mass dampers for multimodal vibration control, *Computers \& Structures,* Vol. 248, pp. 106485, 2021.

[59] A. Toshihiko, Calculation of the H_∞ optimized design of a single-mass dynamic vibration absorber attached to a damped primary system, *Mechanical Engineering Journal,* Vol. 7, No. 5, pp. 20-00250, 2020.

[60] K. Y. T. A. Yoshito Mizukawa, Optimal design of a hysteretically damped dynamic vibration absorber, *Mechanical Engineering Journal,* Vol. 7, No. 2, pp. 19-00482, 2020.

[61] A. K.-J. Marcial Baduidana, Parameters optimization of three-element dynamic vibration absorber with inerter and grounded stiffness, *Journal of Vibration and Control,* Vol. 30, No. 7-8, pp. 1548-1565, 2024.

[62] J. C. J. M. A. A. F.-H. M. A.-M. E. B. Jg Mendoza Larios, A novel high-performance passive non-traditional inerter-based dynamic vibration absorber, *Journal of Sound and Vibration,* Vol. 485, pp. 115583, 2020.